INTERNATIONAL CONGRESS

WAVES AND INSTABILITIES IN PLASMAS

INNSBRUCK, AUSTRIA

SURVEY LECTURES

INSTITUTE FOR THEORETICAL PHYSICS, INNSBRUCK UNIVERSITY
INNSBRUCK, AUSTRIA

INTERNATIONAL CONGRESS

WAVES AND INSTABILITIES IN PLASMAS

Innsbruck, Austria

April 2 - 7 , 1973

SURVEY LECTURES

Editors: G. Auer, F. Cap

Institute for Theoretical Physics,

Innsbruck

Eigentümer, Herausgeber und Verleger im Sinne des Preßgesetzes: Institut für Theoretische Physik, Univ.Prof.F.Cap, Sillgasse 8, 6020 Innsbruck, Austria.

Für den Inhalt verantwortlich: Dr.G.Auer, Dr.F.Cap und die Einzelautoren, Institut für Theoretische Physik, Universität Innsbruck.

DISTRIBUTED by Österreichische Kommissionsbuchhandlung Maximilianstraße 17, A - 6020 Innsbruck, Austria.

NONLINEAR OPTICS OF PLASMAS

Francis F. Chen, Professor of Electrical Sciences

University of California, Los Angeles

I. Introduction

The current interest in high-powered lasers and laser-fusion creates an opportunity to make significant advances in understanding the mechanisms of nonlinear optics. Some nonlinear effects studied in solids and liquids are:

1. Raman and stimulated Raman scattering (SRS)
2. Brillouin and stimulated Brillouin scattering (SBS)
3. Harmonic generation
4. Optical mixing
5. Self-focussing
6. Parametric amplification
7. Electrostriction
8. Induced transparency and opacity

A similar list of nonlinear effects has been predicted for plasmas:

1. Parametric instabilities at $\omega = \omega_p, 2\omega_p$
2. Filamentation (self-focussing)
3. Stimulated Raman scattering
4. Stimulated Brillouin scattering
5. Optical mixing and cascading
6. Double resonance effect
7. Spontaneous magnetic fields
8. Kinetic nonlinear effects

The first five of these may be considered generalizations of the well-known parametric decay instability to situations involving more than one electromagnetic wave, and will be discussed in this light.

Plasmas have several advantages over solid and liquid nonlinear media:

1. Large intensities can be applied to a plasma without danger of destruction of the medium.
2. Different forms and magnitudes of nonlinear susceptibilities can be studied in plasmas than can be found in solids and liquids.
3. New nonlinear saturation mechanisms--e.g. wave breaking and particle trapping--can occur.

4. Effects in plasmas obey purely classical laws, and hence can be predicted by computer simulation.

5. Collisionless wave-particle effects enrich this field of study.

Intense electromagnetic waves can be generated by three types of pulsed lasers, with the following characteristics:

Type	Wavelength (μm)	Frequency (rad/sec)	Cut-off density (cm^{-3})
Nd-glass	1.06	1.8×10^{15}	10^{21}
CO_2	10.6	1.8×10^{14}	10^{19}
HCN	337	5.6×10^{12}	10^{16}

The glass and carbon dioxide lasers can produce powers in excess of 10^9 watts. Although the power achievable with cyanide lasers is presently below 10^3 watts, these can lead to interesting experiments because the cutoff condition ($\omega = \omega_p$) is achieved with a relatively low plasma density. As is well known, the field intensity at a laser focal spot can be awesome. At an intensity $I \equiv c \langle E^2 \rangle / 4\pi$ of 10^{15} W/cm^2, the oscillating electric and magnetic fields have peak values of 9×10^8 V/cm and 3×10^6 G, respectively. The radiation pressure is 3×10^5 atmospheres.

The first seven of the nonlinear effects listed above for a plasma can be described by fluid theory and have a common origin: the $\underline{v} \times \underline{B}$ term in the electron equation of motion

$$m \frac{d\underline{v}}{dt} = -e(\underline{E} + \frac{1}{c} \underline{v} \times \underline{B}). \tag{1}$$

When this last term is neglected, the electrons oscillate in the wave electric field $\underline{E} = \underline{E}_0 \cos \omega t$ with a peak velocity

$$v_0 = eE_0/m\omega \approx 25\, \lambda(\mu) \sqrt{I(W/cm^2)}. \tag{2}$$

For $\lambda = 10.6\mu$, $I = 10^{15}$W/cm^2, as is required for fusion with CO_2 lasers, the value of v_0, called the quiver velocity, corresponds to an electron energy of 16 keV. The magnitude of the nonlinear effect can be estimated by substituting v_0 into the $\underline{v} \times \underline{B}$ term of Eq. (1) and finding $\underline{B}$ from Maxwell's equation

$$c\underline{k} \times \underline{E} = \omega \underline{B}. \tag{3}$$

One then obtains

$$\frac{|\frac{1}{c} \underline{v} \times \underline{B}|}{|\underline{E}|} = \frac{v_0}{c} \equiv \alpha. \tag{4}$$

For $\alpha = 1\%$, the required intensity is $I = 2.5 \times 10^{12}$ W/cm^2 with CO_2 and $I = 2.5 \times 10^{14}$ for Nd-glass lasers. Observable effects are predicted to occur for I at least an order of magnitude lower than this. Note that the required power is not easier to achieve with CO_2 lasers, since the longer wavelength means a larger diffraction limit to the spot size.

We shall confine our attention to phenomena in the absence of an external magnetic field. The subject of nonlinear optics with $\underline{B}_0 \neq 0$ is less well developed and constitutes a rich field of study for the future.

II. The Ponderomotive Force

It turns out that almost all the nonlinear effects listed above can be explained in terms of the so-called ponderomotive force. This effect is most easily derived from the equation of motion (1) for a single electron. Following Schmidt[1], one first solves for the velocity $\underline{v}^{(1)}$ and position $\underline{r}^{(1)}$ of the electron neglecting the $\underline{v} \times \underline{B}$ term. This solution is then used in the next approximation, which takes into account the $\underline{v}^{(1)} \times \underline{B}^{(1)}$ term and the fact that $\underline{E}$ must be evaluated at the actual, rather than the initial, position. Expanding $\underline{E}$ about the initial position, using Eq. (3) for $\underline{B}^{(1)}$, and averaging over time, one obtains

$$m \left\langle \frac{d\underline{v}^{(2)}}{dt} \right\rangle = -\frac{e^2}{m\omega^2} \tfrac{1}{4} (\underline{E}_0 \cdot \nabla \underline{E}_0 + \underline{E}_0 \times \nabla \times \underline{E}_0) \equiv \underline{f}_{NL}. \tag{5}$$

The first term in the nonlinear force $\underline{f}_{NL}$ is a convective term $\underline{v} \cdot \nabla \underline{v}$ related to the longitudinal part of $\underline{E}$; this term is responsible for the electrostatic parametric instabilities discussed in Sec. III. The second term in Eq. (5) concerns the transverse part of $\underline{E}$ and gives rise to the backscattering instabilities of Sec. IV. Part of this term cancels the first term, leaving

$$\underline{f}_{NL} = -\tfrac{1}{4} \frac{e^2}{m\omega^2} \nabla E_0^2. \tag{6}$$

The force per cm^3 is $n_e \underline{f}_{NL}$, where $n_e = m\omega_p^2/4\pi e^2$, and the ponderomotive force is

$$\underline{F}_{NL} = -\frac{\omega_p^2}{\omega^2} \nabla \frac{\langle E^2 \rangle}{8\pi} \tag{7}$$

Although the force on the ions is weaker by m/M, the ponderomotive force on the electrons is communicated to the massive ions by the charge-separation electric field, as long as the motions are of low frequency.

Eq. (7) can also be derived[2,3] from the Maxwell stress tensor for a medium with a dielectric constant $\varepsilon = 1-\omega_p^2/\omega^2$. Although the radiation pressure $\nabla\langle E^2/8\pi\rangle+\nabla\langle B^2/8\pi\rangle$ does not contain ω_p explicitly, these two terms normally cancel in a vacuum. In a plasma, the electron motions cause the cancellation to be inexact, and the resulting force is proportional to $\varepsilon-1 = \omega_p^2/\omega^2$. The physical mechanism is clearer from the single-particle point of view: the electrons suffer a secular drift because of the distortion of their orbits by the wave magnetic field or because their excursions take them into regions of different field strength.

The ponderomotive force has several direct effects. In an inhomogeneous plasma, a wave entering along the density gradient will have a standing wave pattern (Fig. 1) which increases in amplitude near the cutoff region ($\omega_p \approx \omega$). This well-known Airy-function pattern[4] has a large gradient of E^2 near cutoff, and the ponderomotive force can cause ion motions. By modulating the incident

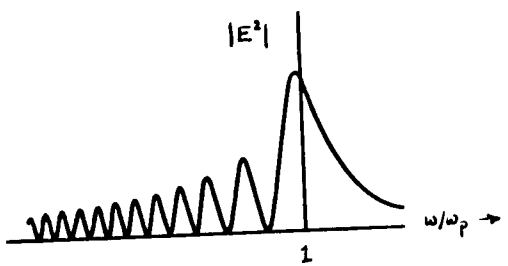

Fig. 1.

wave at an ion frequency, low-frequency waves can be excited or feedback-stabilized. This is the so-called double-resonance effect[5]. Since $\underline{F}_{NL}$ changes sign in each cycle of the standing wave, the plasma tends to become stratified by very large amplitude waves, as has been "observed" in computer simulations[6].

In a homogeneous plasma there can still be a gradient of E^2 if the laser beam has finite radius (Fig. 2). The ponderomotive force is radially outward,

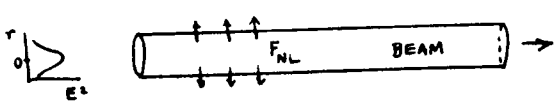

Fig. 2.

causing a decrease in plasma density inside the beam. Self-focussing occurs when the ensuing change in index of refraction acts back on the beam to focus it to a smaller diameter. Although the ponderomotive force has been detected in microwave experiments and self-focussing has been observed in liquids and in plasmas[7], there has been no direct verification of Eq. (7) for a plasma.

III. "Ordinary" Parametric Instabilities

1. Oscillating two-stream (OTS) instability. The electrostatic parametric instabilities extensively studied in both the laboratory and the ionosphere[8] are divided into two types, depending on the sign of $\omega_0-\omega_p$. [For finite temperatures, ω_p is to be replaced by the Bohm-Gross frequency ω_e, given by $\omega_e^2 = \omega_p^2+3k^2v_e^2$.] The reason for this difference is easily seen from the ponderomotive force[8]. If $\omega_0 < \omega_p$, one has the OTS instability, in which density ripples in the direction of E_0 grow without propagation (Fig. 3). Let a quasineutral density perturbation n_1 have $k >> k_0$, so that k_0 can be

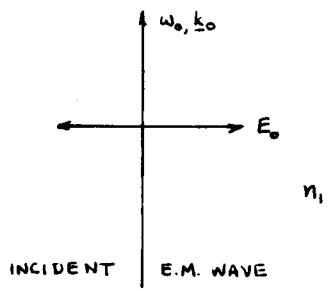

Fig. 3.

assumed to vanish. The motion of electrons in the direction of $-\underline{E}_0$ will give rise to a space charge oscillating at frequency ω_0, as shown in Fig. 4.

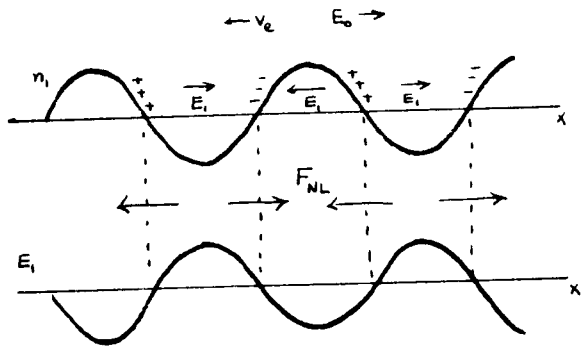

Fig. 4.

This space charge creates a field $\underline{E}_1$ with the phase shown in Fig. 4. For uniform $\underline{E}_0$, the ponderomotive force is given by

$$8\pi \frac{\omega^2}{\omega_p^2} \underline{F}_{NL} = -\nabla(\underline{E}_0+\underline{E}_1)^2 \simeq -2\underline{E}_0\cdot\nabla\underline{E}_1 = -2E_0 \frac{\partial E_1}{\partial x} \qquad (8)$$

and hence has the phase shown in Fig. 4. Since $\underline{F}_{NL}$ acts to move plasma into the regions of positive n_1, the density perturbation grows. This is an absolute instability with $\mathrm{Re}\omega = 0$. Although these phase relationships hold for any $\omega_0 < \omega_e$, excitation is easiest when ω_0 is near the natural oscillation frequency ω_e. The electrons move in a standing wave, but the ion motion does not follow a natural mode of the ion fluid.

2. Parametric decay instability. If ω_0 is larger than ω_e, the OTS mechanism does not work; instead, the incident wave decays into an electron wave ω_e and an ion acoustic wave $\omega_i = kc_s$. Consider an oscillator x with natural frequency ω_e driven by a force $F\cos\omega_0 t$:

$$\ddot{x} + \omega_e^2 x = F\cos\omega_0 t, \qquad x = \frac{F\cos\omega_0 t}{\omega_e^2-\omega_0^2} \quad . \qquad (9)$$

If $\omega_0 < \omega_e$, the displacement is in the same direction as the force, and the mechanism of Fig. 4 obtains. If $\omega_0 > \omega_e$, the displacement, and therefore F_{NL}, has the opposite sign; and a static density perturbation would decay. However, if the density ripple is an ion wave traveling with velocity c_s, the electron fluid can feel a frequency $\omega_0' \lesssim \omega_e$ in the Doppler-shifted frame, and the previous mechanism can operate in that frame. The requirement $\omega_0' = \omega_0 - kc_s \lesssim \omega_e$ is just the frequency-matching condition $\omega_0 = \omega_e+\omega_i$. Fig. 5A shows the usual parallelogram construction for ω and k matching in the parametric decay instability.

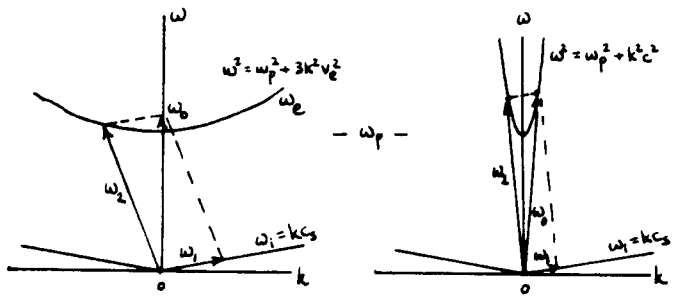

(A) DECAY INSTABILITY (B) BACKSCATTERING INSTABILITY

Fig. 5.

IV. Backscattering Instabilities

1. Introduction. Fig. 5B shows the ω and k matching condition for the parametric decay of an electromagnetic wave ω_0 into an electrostatic wave ω_1, in this case an ion wave, and another electromagnetic wave ω_2 in the opposite direction. This interaction has received recent attention because of the possibility of reflection of laser radiation in the outer, underdense layers of a plasma created by the laser, rather than absorption near the critical layer by the processes of Sec. III. In the most likely process, the backscattered wave is exactly opposite to the incident wave, and the matching conditions are $\omega_0 = \omega_1+\omega_2$, $\underline{k}_0 = \underline{k}_1+\underline{k}_2 = (|k_1|-|k_2|)(\underline{k}_0/k_0)$. We shall illustrate the case $\omega_0 >> \omega_p$ (Fig. 6), where $\underline{k}_2 \approx -\underline{k}_0$, and therefore $\underline{k}_1 \approx 2\underline{k}_0$.

2. Physical mechanism. Let the incident wave be $E_0\hat{x}\cos(\omega_0 t - k_0 y)$. The quiver velocity

$$\underline{v}_0 = -\frac{eE_0}{m\omega_0}\sin(\omega_0 t - k_0 y)\hat{x} \qquad (10)$$

then leads E_0 by 90°.

Fig. 6.

We look for a ponderomotive force F_{NL} at the relatively low frequency ω_1 of the plasma wave, caused by beats between the incident wave ω_0 and the backscattered wave ω_2. The first term in the analog of Eq. (5) vanishes by geometry, and the second term gives

$$\underline{F}_{NL} = -en_0(\underline{v}_2 \times \underline{B}_0 + \underline{v}_0 \times \underline{B}_2). \qquad (11)$$

Fig. 7A shows the phase of the $-\underline{v}_2 \times \underline{B}_0$ term at an instant of time when E_0 and the quiver velocity v_2 of the scattered wave are in phase. Fig. 7B shows the situation ¼ of a period later. The $-\underline{v}_2 \times \underline{B}_0$ term, shown by the thick arrows, oscillates between 0 and the peak value in the direction shown (depending on position), and hence has a finite average over the fast time scale of ω_0.

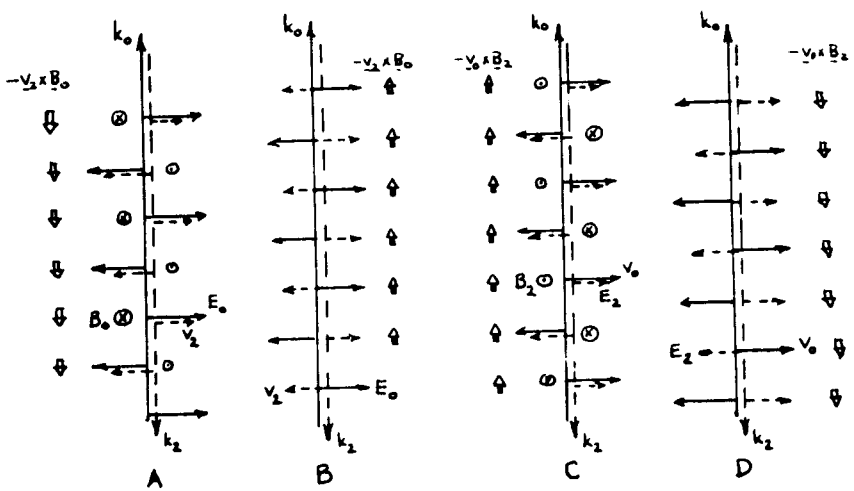

Fig. 7

Since $\underline{v}$ leads $\underline{E}$ by 90°, one obtains Figs. 7C and 7D for the phases of the $-\underline{v}_0 \times \underline{B}_2$ term at the times corresponding to Figs. 7A and 7B, respectively. It is seen that the two terms in F_{NL} add in phase in such a way as to cause electrons to bunch up and form a density ripple with half the wavelength of the electromagnetic waves ($k_1 = 2k_0$). Thus, a density perturbation n_1 (Fig. 8) results from the nonlinear interference of the incident and backscattered waves.

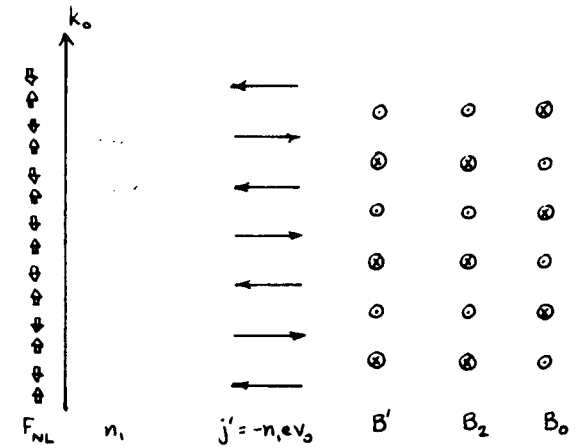

Fig. 8

It remains to show that n_1 causes the wave ω_2 to grow at the expense of the wave ω_0, and hence there is instability. Since $\underline{v}_0$ is perpendicular to ∇n_1, we do not have the charge separation mechanism of the OTS instability. Instead, the effect is a spatial modulation of the oscillating current $-ne\underline{v}_0$ caused by $\underline{v}_0$. Let us neglect the motion of the density ripples and consider a phase 1/8 of a period after that of Fig. 7C. The maxima of $\underline{v}_0$ and n_1 are then aligned, and the current modulation $\underline{j}' = -n_1 e\underline{v}_0$ is as shown in Fig. 8. This current drives a magnetic field B' with the phase shown. At this instant of time, the phases of B_2 and B_0 are as shown. It is seen that B' is in phase with B_2 and out of phase with B_0. Thus, $\underline{j}'$ excites the backscattered wave at the expense of the

incident wave.

The density perturbation may or may not be a natural mode of the plasma, but is naturally more easily excited in the former instance. We distinguish three cases:

A) If $\omega_1 = \omega_e$ (an electron plasma wave), the process is called stimulated Raman scattering (SRS).

B) If $\omega_1 = kc_s$ (an ion acoustic wave), the process is called stimulated Brillouin scattering (SBS).

C) If ω_1 does not correspond to a normal mode, the process is called resistive quasimode scattering. The density perturbation must be maintained against diffusion, but the process may be important because of the large range of ω_1 possible[9].

3. Results for homogeneous plasma. In a homogeneous plasma the thresholds and linear growth rates for the SBS and SRS processes can be calculated from the general theory of Nishikawa[10]. The results, which are well known[9,11-14] although difficult to find in print, are approximately as follows.

	Threshold	Growth Rate	
SBS	$\frac{v_0^2}{v_e^2} = \frac{8\gamma_i \nu_{ei}}{\omega_i \omega_0}$	$\gamma \approx \frac{1}{2}\frac{v_0}{c}(\omega_0/\omega_i)^{1/2}\omega_{pi}$	(12)
SRS	$\frac{v_0^2}{c^2} = \frac{2\omega_p^2}{\omega_0^2}\frac{\gamma_e}{\omega_p}\frac{\nu_{ei}}{\omega_0}$	$\gamma \approx \frac{1}{2}\frac{v_0}{c}(\omega_0\omega_p)^{1/2}$	(13)

Here v_e is the electron thermal speed, γ_i and γ_e are the damping rates of the ion or electron wave, and $\frac{1}{2}\nu_{ei}\omega_p^2/\omega_0^2$ is the damping rate of the electromagnetic waves. These collisional thresholds are exceedingly low, even for SRS -- typically, $I \gtrsim 10^7$ W/cm^2 for CO_2. The growth rates are appreciable, and depend only weakly on density. If these values were relevant, anomalous reflection from underdense plasmas would have been observed long ago. However, there are complications.

4. Finite length effect. If the interaction region is limited in length d by either the depth of focus of the laser or the plasma size, the growth rate must be large enough to overcome the loss of wave energy by convection out of the region. The backscattered wave starts at the far end at thermal level and grows as it travels toward the laser at a group velocity $\approx c$. The plasma wave starts at the near end at thermal level and grows as it travels downstream with the group velocity v_g. It turns out that for a normal mode it is the geometric mean that matters, and the condition for appreciable growth is

$$\gamma \gg \sqrt{cv_g}/d \quad , \tag{14}$$

where γ is the linear growth rate given above. The detailed treatment of the spatially varying problem[11,13] has many subcases, but Eq. (14) has wide applicability.

5. Plasma inhomogeneity. If the plasma is infinite but inhomogeneous, a different effect occurs. The plasma wave has a different wavelength in each part of the plasma, so that the backscattered wave, which has a nearly fixed wavelength if the plasma is quite underdense, can maintain the correct phase relationship with the plasma wave only over a finite length. Growth occurs only in this region; there is pure oscillation outside. The backscattered intensity grows by a factor[15,13]

$$I/I_0 = \exp(2\pi\gamma^2/cv_g k') \quad , \tag{15}$$

where $k' = dk/dx$. In SRS, it is the density gradient length L_n which matters, since the Bohm-Gross dispersion relation is sensitively dependent on ω_p. In SBS, it is the temperature gradient length L_T which is important in the ion wave dispersion relation. Using these relations and the values of γ from Eqs. (12) and (13), one obtains the following "inhomogeneous thresholds" from Eq. (15):

SBS
$$\frac{v_0^2}{v_e^2} > \frac{\omega_0^2}{\omega_p^2}\frac{8}{k_0 L_T} \tag{16}$$

SRS
$$\frac{v_0^2}{c^2} > \frac{2}{k_0 L_n} \quad . \tag{17}$$

The space and time behaviors of the perturbations are interlinked in a complicated way[13]. Note that the density dependence has cancelled out in Eq. (17). SRS can occur in a very underdense plasma because although the growth rate is small, so is the phase mismatch. In a finite, inhomogeneous plasma, Eq. (17) is likely to be the controlling condition for SRS and Eq. (14) for SBS.

6. Finite linewidth. If the laser beam has a frequency spread $\Delta\omega$, the resulting phase mixing can greatly reduce backscattering. This has been shown in numerical computations[16] and in experiment[17].

7. Convective and absolute instabilities. In the theory of beam-plasma instabilities, convective and absolute instabilities can be distinguished by the behavior of the dispersion curve near the intersections of the uncoupled modes. In backscattering, the relevant uncoupled modes are the electrostatic wave $\omega_1, \underline{k}_1$ and the difference wave $\omega_0-\omega_2$, $\underline{k}_0-\underline{k}_2$. Fig. 9 shows

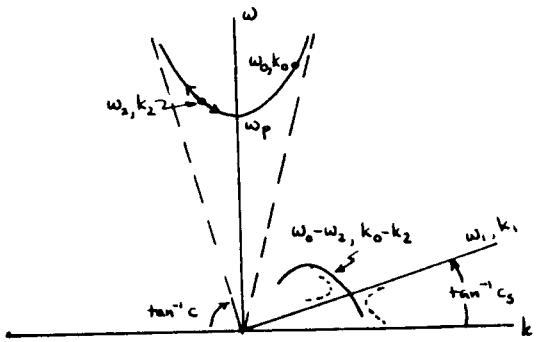

Fig. 9.

the specific situation of Fig. 5B, in which $\omega_1 = k_1 c_s$ (SBS). As the point ω_2, k_2 is moved along the curve $\omega^2 = \omega_p^2 + k^2c^2$ with ω_0, k_0 fixed, the curve $\omega_0-\omega_2$, k_0-k_2 is traced out. Instability occurs near synchronism with the ion wave ω_1, k_1. Because the group velocities are oppositely directed, the instability is absolute, as is indicated by the shape of the coupled dispersion relation (dashed curve), with complex ω for real k. This holds in the absence of dissipation. With damping, the Bers-Briggs analysis[18] must be made with complex ω. The result[19] is that there is a convective instability with a lower threshold than that for the absolute instability. The OTS and filamentation instabilities are intrinsically absolute and do not have a convective counterpart. This analysis[19] has been made only for an infinite plasma; but, of course, it is in a finite medium that convection is important.

8. Nonlinear saturation. Current interest is centered on the nonlinear behavior of these instabilities, since this determines their practical importance. Analysis of the nonlinear regime[11] shows that the growth rate (both temporal and spatial) varies with amplitude in the manner shown in Fig. 10.

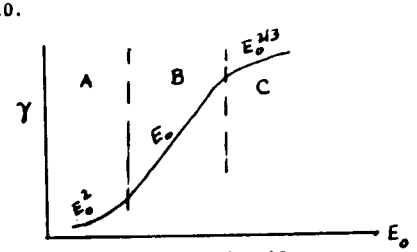

A: resistive quasimodes
B: normal modes
C: reactive quasimodes

Fig. 10.

Region B is the region of linear growth as given by Eqs. (12) and (15). At lower intensities (Region A), the plasma waves are damped by collisions, but density perturbations which do not follow a dispersion relation but simply diffuse can be excited. At high intensities (Region C), the ponderomotive force term affects the frequency of the plasma waves, and the growth rate varies as $E_0^{2/3}$. This dependence at high intensity is quite general for parametric instabilities[10].

Possible saturation mechanisms for SRS are electron trapping, heating followed by increased Landau damping, mode-coupling with nonlinear Landau damping, and modulational instabilities[14]. The last mechanism is the refraction of plasma waves away from regions of high density because the index of refraction for them is less than unity. The waves then pile up in regions of low density, and the ponderomotive force causes the density to decrease further there. The large density perturbations have a stabilizing influence because of Eq. (17). Ion waves are not subject to these saturation mechanisms, and consequently SBS is expected to have large amplitudes. This is borne out by numerical simulations carried out at Los Alamos[11] and Livermore[16]. These one-dimensional computations with a linear density profile show that (1) SRS occurs first, because of the larger growth rate, but then decays as electrons get trapped and the waves break; (2) SRS reflects at most 50% of the incident energy; (3) SBS starts later but reaches large amplitude; (4) there are relaxation oscillations in the reflected power, which can reach 99% for appreciable periods; (5) the light eventually pushes its way through any finite slab of plasma. These results are for $\omega_0 \gtrsim$ 10-100 ω_p. For $\omega_0 = 2\omega_p$, a very strong instability develops which effectively splits the plasma at that point. This is because the backscattered wave then has frequency ω_p and cannot propagate out of the plasma.

V. Sidescattering and Filamentation

Consider now the orientation of wave vectors as the angle between $\underline{k}_1$ and $\underline{k}_0$ is changed, as in Fig. 11. Since $|k_2|$ is fixed at $\simeq\omega_0/c$, the locus

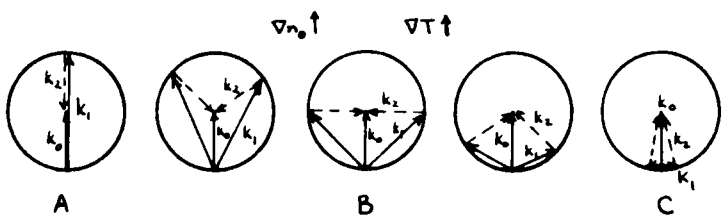

Fig. 11

of the tip of the $\underline{k}_1$ vector lies on a circle. Fig. 11 is for the case $\omega_2 = \omega_0 - \omega_1$, $\underline{k}_2 = \underline{k}_0 - \underline{k}_1$ which we have been discussing. The corresponding diagrams for $\omega_2 = \omega_0 + \omega_1$, $\underline{k}_2 = \underline{k}_0 + \underline{k}_1$ would have the $\underline{k}_1$ arrow in the opposite direction. The latter case is not important for scattering (since $\omega_2 > \omega_0$) but will have to be considered for filamentation (where $\mathrm{Re}\omega_1 = 0$). Case (A) above is backscattering. Case (C) is forward scattering; this is a weak interaction because $\underline{k}_1$, and hence the electrostatic field, is small. Case (B), sidescattering, is important because $\underline{k}_2$ is perpendicular to the gradients in n_0 and T if $\underline{k}_0$ enters the plasma at normal incidence; consequently, the phase mismatch due to plasma inhomogeneity is absent, and the growth rate is limited only by the finite beam radius a (cm) and damping rate γ_1. For SRS, Kaufman et al.[20] calculate the threshold intensities for CO_2 to be

$$\text{sidescattering:} \quad I_s > 4.5\, G_s\, \gamma_1/\omega_p a \times 10^{12} \mathrm{W/cm}^2 \tag{18}$$

$$\text{backscattering:} \quad I_b > 0.7\, G_b/L_n \times 10^{12} \mathrm{W/cm}^2 \ , \tag{19}$$

where $G_s \approx 35$ and $G_b \approx 30$ are the required number of e-foldings of growth from thermal fluctuations. Eq. (19) is the same as Eq. (17) for $G_b = 2\pi$. Thus, depending on the ratio a/L_n, sidescattering may be as important as backscattering. Fig. 12 shows the physical mechanism. The wave fronts

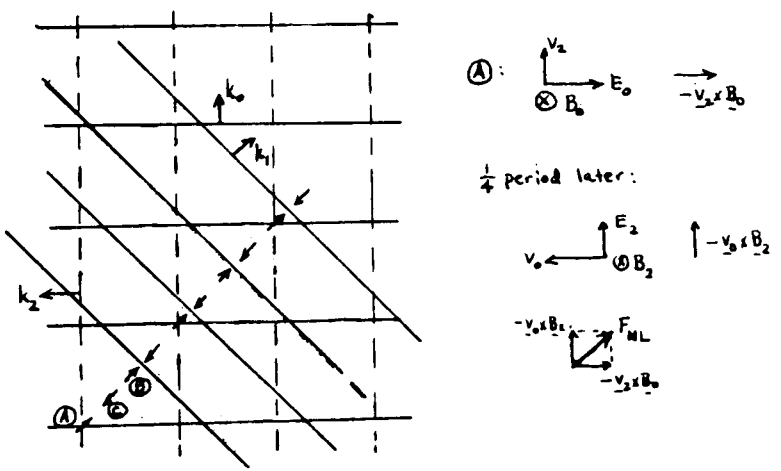

Fig. 12.

of the incident wave $\underline{k}_0$ and the scattered wave $\underline{k}_2$ (traveling to the left) are shown. At the point A, $\underline{E}_0$ and $\underline{v}_2$ are at their maxima; the force $-e\underline{v}_2\times\underline{B}_0$ is then to the right. A quarter period later, $\underline{v}_0$ and $\underline{E}_2$ are in phase at the same point A, giving rise to an equal force $-e\underline{v}_0\times\underline{B}_2$ directed upward. The time-averaged force $\underline{F}_{NL}$ at A is therefore at 45° to $\underline{k}_0$. The $\underline{E}_0\cdot\nabla\underline{E}_2 + \underline{E}_2\cdot\nabla\underline{E}_0$ part of Eq. (5) is in the opposite direction, diminishing the effect. At the point B, both $\underline{v}$ and $\underline{E}$ are reversed in direction, so that $\underline{F}_{NL}$ is as at A. At C, $\underline{v}$ and $\underline{E}$ are shifted 90° from A in opposite directions, so that their product, and therefore F_{NL}, is the negative of that at A. The resulting pattern of the ponderomotive force causes density striations at 45°, in agreement with Fig. 11B. Note that the regular spacing of the density ripples is possible in SRS only if $\omega = \omega_p$ (cold plasma). For finite temperature, the relation $\omega_1^2 = \omega_p^2 + 3k_1^2 v_e^2$ requires k_1 to vary if ω_p does, and phase mismatches occur even in sidescattering.

Filamentation, or self-focussing, occurs when the incident wave vector lies along incipient density striations (Fig. 13). The refraction caused by

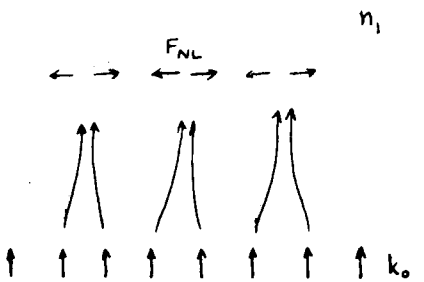

Fig. 13.

the density perturbations cause the light beam to be channeled into the less dense regions. The resulting ponderomotive force pushes plasma away from such regions and increases the density perturbation. If $\underline{F}_{NL}$ is large enough to overcome the plasma pressure, the instability grows at the rate[9] $\gamma \approx (v_0/c)\omega_{pi}$. For a Gaussian beam, the self-focussing threshold is[21]

$$P_c = 8500(\omega_0/\omega_p)^2 (KT)_{eV} \text{ watts} \tag{20}$$

Note that it is the total power P_c, not the intensity, which matters.

Filamentation may be considered a parametric decay in which the ion wave $\underline{k}_1$ is at right angles to $\underline{k}_0$ (Fig. 11C). Since $\underline{k}_1$ is small in this limit, the process $\underline{k}_2 = \underline{k}_0 + \underline{k}_1$ is indistinguishable from $\underline{k}_2 = \underline{k}_0 - \underline{k}_1$; and both must be considered. This is, therefore, a four-wave, rather than a three-wave,

interaction. The forward-scattered waves $\underline{k}_2$ interfere with the incident wave to produce the self-focussing. The geometry of this instability is identical with that of the OTS instability (Fig. 3), and both are non-convective. However, since $\underline{k}_2$ is a light wave, the simplification $k_0 \ll k_1$ cannot be made in filamentation.

An equilibrium density distribution exists in which

$$n = n_0 \exp[e(\phi+\phi_{NL})/kT_e] \quad , \tag{21}$$

where $\phi_{NL} = -(\omega_p^2/\omega_0^2)\langle E^2\rangle/8\pi e n_0$. As the intensity is increased, the filaments break up into smaller and smaller ones until the minimum radius c/ω_p (the collisionless skin depth) is reached[22]. The stability of these equilibria is unknown.

VI. Optical Mixing and Cascading

By using two lasers with a frequency difference, it is possible to couple strongly to an underdense plasma by making $\omega_0-\omega_1 = \omega_p$. This was first suggested by Kroll, Ron, and Rostoker[23] and experimentally tested by Stansfield, Nodwell, and Meyer[24]. Recent work[25,26,27] treats nonlinear saturation and plasma inhomogeneity. Fig. 14 illustrates the basic idea. In the Raman process, two electromagnetic pump waves ω_0 and ω_2 beat with each

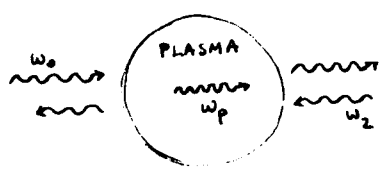

Fig. 14.

other to generate a plasma wave ω_1, such that $\omega_0-\omega_2 = \omega_1 \tilde{=} \omega_p$, $\underline{k}_0-\underline{k}_2 = \underline{k}_1 \tilde{=} 2\underline{k}_0$. The plasma wave, in turn, interacts with the incident waves to change their amplitudes: the higher-frequency wave ω_0 is damped, while the lower-frequency wave ω_2 is enhanced. The interaction is strongest with $\underline{k}_2 = -\underline{k}_0$, as shown. This process will be recognized as just stimulated backscattering: the backscattered wave ω_2, with the proper frequency shift, is imposed on the plasma, so that it does not have to grow from thermal noise. The threshold, therefore, is lower than in SRS. The theory differs only in that the amplitude of ω_2 is assumed fixed, with the consequence that the ω_p oscillation grows linearly with time rather than exponentially.

It is tempting to try to heat a plasma by this anomalous absorption process. For instance, the 10.6μ and 10.2μ lines of the CO_2 laser can beat to couple with a plasma of density 1.5×10^{16} cm^{-3}, or the 10.6μ and 9.6μ lines with $n = 10^{17}$cm^{-3}. Unfortunately, the energy given to the wave ω_1 is much less than the energy exchange between ω_0 and ω_2. This is a consequence of the conservation of action. From a quantum mechanical viewpoint, the energy of a wave is $W = N\hbar\omega$, where N is the number of quanta. Since N is conserved, one has

$$\frac{W_0}{\omega_0} = \frac{W_1}{\omega_1} = \frac{W_2}{\omega_2} \quad , \tag{22}$$

where W_1 is small because $\omega_1 \ll \omega_0,\omega_2$. However, the wave momenta $\underline{p} = N\hbar\underline{k}$ are such that they add rather than subtract, and electromagnetic momentum can be transferred to the plasma to achieve low-frequency coupling.[27]

To circumvent the restriction on energy coupling, Kaufman et al.[28] suggested a cascade process (Fig. 15). Two incident beams $\omega_0,\underline{k}_0$ and

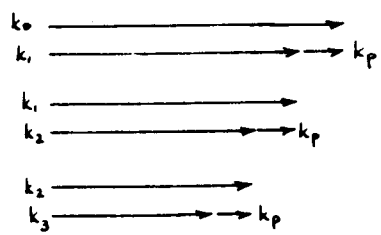

Fig. 15.

$\omega_1,\underline{k}_1$ undergo forward scattering to produce a plasma wave $\omega_p = \omega_0-\omega_1$, $\underline{k}_p = \underline{k}_0-\underline{k}_1$. The plasma wave then interacts with $\underline{k}_1$ to produce $\omega_2 = \omega_1-\omega_p$, $\underline{k}_2 = \underline{k}_1-\underline{k}_p$, and so forth until the laser energy is almost all converted into plasma waves. Repeated k-matching, unfortunately, works only for forward scattering, which is ω_p/ω_0 times less efficient than backscattering. Because of this, the threshold for cascading is rather high. At $I = 2 \times 10^{14}$W/cm^2 for CO_2, energy absorption is about 50% in a 10 cm length. By contrast, optical mixing with opposing beams[28] gives 90% energy exchange between beams at $I = 6 \times 10^{11}$W/cm^2.

VII. Conclusion

We cannot also review at this time the kinetic nonlinear theories pioneered by J.M. Dawson, nor the work of our Soviet colleagues, nor the available experimental results. In any case, definitive experiments have yet to be done; theory is more advanced than experiment at this moment. We hope that this situation can be reversed in the near future.

We are grateful to a large number of authors for discussing their unpublished results. Above all, we wish to thank Prof. George Schmidt, without whose guidance and physical insight this work would have been impossible. This work was supported by the U.S. Atomic Energy Commission under Contract AT(04-3)-34, Project 157.

REFERENCES

1. G. Schmidt, Physics of High Temperature Plasmas (Academic Press, New York, 1966), p. 47ff.
2. J.W. Shearer and J.L. Eddleman, Lawrence Livermore Laboratory, UCRL-73969 (1972), submitted to Physics of Fluids.
3. R.E. Kidder, Lawrence Livermore Laboratory, UCRL-74040 (1972), Japan-U.S. Seminar on Laser Interaction with Matter, Kyoto, 1972.
4. V.L. Ginzburg, Propagation of Electromagnetic Waves in Plasmas, (Pergamon Press, New York, 1964), p. 365.
5. A.Y. Wong, F.F. Chen, N. Booth, D.L. Jassby, R. Stenzel, D. Baker, and C.S. Liu, Plasma Physics and Controlled Nuclear Fusion Research, (International Atomic Energy Agency, Vienna, 1971), p. 335.
6. J.S. de Groot, unpublished.
7. A.J. Alcock, Laser Interaction and Related Plasma Phenomena, ed. by H.J. Schwarz and H. Hora (Plenum Press, New York, 1972) Vol. 2, p. 155.
8. A.Y. Wong and G. Schmidt, UCLA PPG-151 (1973).
9. J. Drake, P. Kaw, Y.C. Lee, G. Schmidt, C.S. Liu, and M. Rosenbluth, UCLA PPG-158 (1973).
10. K. Nishikawa, J. Phys. Soc. Japan 24, 916 (1968).
11. D.W. Forslund, J.M. Kindel, and E.L. Lindman, to be published; also Phys. Rev. Lett. 30, 739 (1973).
12. C.S. Liu and M.N. Rosenbluth, to be published.
13. D. Pesme, G. Laval and R. Pellat, Phys. Rev. Lett. 31, 203 (1973).
14. M.N. Rosenbluth and R.Z. Sagdeev, Comments on Plasma Physics and Controlled Fusion 1, 129 (1972).
15. M.N. Rosenbluth, Phys. Rev. Lett. 29, 565 (1972).
16. W. Kruer, Lawrence Livermore Laboratory (private communication).
17. C. Yamanaka, Proc. of the U.S.-Japan Seminar on Laser Interaction with Matter, Kyoto, 1972.
18. R.J. Briggs, Electron-Stream Interaction with Plasmas (MIT Press, 1964).
19. B.D. Fried, R.W. Gould, and G. Schmidt, UCLA PPG-146 (1973).
20. M.A. Mostrom, D.R. Nicholson, and A.M. Kaufman, Lawrence Berkeley Laboratory, LBL-2032 (1973).
21. J.W. Shearer and J.L. Eddleman, Lawrence Livermore Laboratory UCRL-73969 (1972).
22. P. Kaw, G. Schmidt, and T. Wilcox, UCLA PPG-140 (1972).
23. N.M. Kroll, A. Ron, and N. Rostoker, Phys. Rev. Lett. 13, 83 (1964).
24. B.L. Stansfield, R. Nodwell, and J. Meyer, Phys. Rev. Lett. 26, 1219 (1971),
25. M.N. Rosenbluth and C.S. Liu, Phys. Rev. Lett. 29, 701 (1972).
26. G. Schmidt, UCLA PPG-133 (1972).
27. F.F. Chen, Comments on Plasma Physics and Controlled Fusion 1, 81, (1972).
28. B.I. Cohen, A.N. Kaufman, and K.M. Watson, Phys. Rev. Lett. 29, 581 (1972).
29. A.N. Kaufman and B.I. Cohen, Phys. Rev. Lett. 30, 1306 (1973).